remote sensing

MDPI

Article

Long-Term Spatiotemporal Variability and Source Attribution of Aerosols over Xinjiang, China

Chenggang Li [1], Xiaolu Ling [1,2,*], Wenhao Liu [1], Zeyu Tang [1], Qianle Zhuang [3] and Meiting Fang [1]

[1] School of Environment and Spatial Informatics, China University of Mining and Technology, Xuzhou 221116, China; ts23160015a31@cumt.edu.cn (C.L.); tb21160015b1@cumt.edu.cn (W.L.); ts22160044a31@cumt.edu.cn (Z.T.); ts24160152p31@cumt.edu.cn (M.F.)
[2] Jiangsu Key Laboratory of Coal-Based Greenhouse Gas Control and Utilization, China University of Mining and Technology, Xuzhou 221008, China
[3] Natural Resources Comprehensive Investigation and Monitoring Institute of Qinghai Province, Xining 810001, China; zhuangqianle6175@163.com
* Correspondence: lingxl@cumt.edu.cn

Abstract

Aerosols play a critical role in modulating the land–atmosphere energy balance, influencing regional climate dynamics, and affecting air quality. Xinjiang, a typical arid and semi-arid region in China, frequently experiences dust events and complex aerosol transport processes. This study provides a comprehensive analysis of the spatiotemporal evolution and potential source regions of aerosols in Xinjiang from 2005 to 2023, based on Moderate Resolution Imaging Spectroradiometer (MODIS) aerosol products (MCD19A2), Cloud-Aerosol Lidar and Infrared Pathfinder Satellite Observation (CALIPSO) vertical profiles, ground-based $PM_{2.5}$ and PM_{10} concentrations, MERRA-2 and ERA5 reanalysis datasets, and HYSPLIT backward trajectory simulations. The results reveal pronounced spatial and temporal heterogeneity in aerosol optical depth (AOD). In Northern Xinjiang (NXJ), AOD exhibits relatively small seasonal variation with a wintertime peak, while Southern Xinjiang (SXJ) shows significant seasonal and interannual variability, characterized by high AOD in spring and a minimum in winter, without a clear long-term trend. Dust is the dominant aerosol type, accounting for 96.74% of total aerosol content, and AOD levels are consistently higher in SXJ than in NXJ. During winter, aerosols are primarily deposited in the near-surface layer as a result of local and short-range transport processes, whereas in spring, long-range transport at higher altitudes becomes more prominent. In NXJ, air masses are primarily sourced from local regions and Central Asia, with stronger pollution levels observed in winter. In contrast, springtime pollution in Kashgar is mainly influenced by dust emissions from the Taklamakan Desert, exceeding winter levels. These findings provide important scientific insights for atmospheric environment management and the development of targeted dust mitigation strategies in arid regions.

Keywords: aerosols; aerosol source; spatiotemporal patterns; backward trajectory; CWT

check for updates

Academic Editor: Carmine Serio

Received: 12 May 2025
Revised: 18 June 2025
Accepted: 24 June 2025
Published: 26 June 2025

Citation: Li, C.; Ling, X.; Liu, W.; Tang, Z.; Zhuang, Q.; Fang, M. Long-Term Spatiotemporal Variability and Source Attribution of Aerosols over Xinjiang, China. *Remote Sens.* **2025**, *17*, 2207. https://doi.org/10.3390/rs17132207

Copyright: © 2025 by the authors. Licensee MDPI, Basel, Switzerland. This article is an open access article distributed under the terms and conditions of the Creative Commons Attribution (CC BY) license (https://creativecommons.org/licenses/by/4.0/).

1. Introduction

Aerosols refer to solid or liquid particles suspended in the atmosphere, originating from both natural processes such as wind-blown dust and volcanic eruptions, as well as human activities, including industrial emissions and fossil fuel combustion. Aerosols influence the Earth's radiative balance by absorbing and scattering solar radiation [1]. Additionally, aerosols can serve as cloud condensation nuclei or ice nuclei, thereby affecting

cloud formation and precipitation processes [2]. Aerosols can persist in the atmosphere from hours to weeks. Driven by atmospheric circulation, meteorological conditions, and topography, they undergo interregional transport and redistribution [3], with significant impacts on local and global air quality, climate change, human health, and ecosystems [4–7]. Aerosols consist of suspended particles ranging in size from nanometers to tens of micrometers and are ubiquitously distributed throughout the atmosphere. Based on particle size, atmospheric particulate matter is typically classified as inhalable particulate matter (PM_{10}, particles smaller than 10 μm) and fine particulate matter ($PM_{2.5}$, particles smaller than 2.5 μm). Both $PM_{2.5}$ and PM_{10} are important indicators of air quality, and there is a significant correlation between them and aerosol optical depth (AOD). Therefore, $PM_{2.5}$ and PM_{10}-$PM_{2.5}$ ($PM_{10–2.5}$) are commonly used as typical indicators of fine and coarse aerosols for research purposes [8,9].

A large body of research has focused on the sources and transport of aerosols, with study areas primarily concentrated in regions such as Central Asia, the Sahara Desert, and the Australian Outback [10–12]. Previous studies have indicated that the primary type of aerosol in Central Asia is dust aerosol, mainly originating from the Taklimakan Desert and the Gobi Desert in Inner Mongolia. During transboundary dust transport in Asia, approximately 30% of the dust is redeposited over desert regions, while 20% is transported on regional scales. Some of the dust travels through the Hexi Corridor and the Loess Plateau to reach southeastern China. The remaining 50% enters the westerly wind belt, disperses globally, and can ultimately be transported from the continent to the open seas near Korea and Japan, even reaching eastern North America [13–15]. The sources of aerosols in Central Asia exhibit clear seasonal characteristics, with aerosols in spring and summer primarily coming from external transport, whereas aerosols in autumn and winter are mostly derived from local emissions [16]. Under the influence of the westerlies, aerosol events in Central Asia are most frequent in spring, with transport often further influenced by low-pressure systems, which enhance the long-range transport capacity and spatial diffusion of aerosols [17]. Long-range transport not only affects the local climate and environment but also enhances boundary layer stability, which in turn exacerbates pollutant accumulation and contributes to persistent pollution episodes [18].

Xinjiang is the land-based core of the Belt and Road Initiative's western extension and acting as a 'golden passage' connecting China to Central Asia, Western Asia, and even Europe. Xinjiang is home to deserts such as the Taklamakan and the Gurbantünggüt, characterized by an arid climate, low precipitation, sparse vegetation, and strong winds, leading to frequent dust storms every year [19], which result in the emission of large amounts of dust aerosols into the atmosphere [20]. In addition to the widespread natural dust sources, Xinjiang also faces anthropogenic pollution sources such as industrial emissions and transportation. The combined effects of natural and anthropogenic sources make the aerosol types more complex, with chemical composition and optical properties showing significant regional heterogeneity, thereby having a substantial impact on the atmospheric environment and climate system [21]. Previous studies on aerosols have primarily focused on satellite remote sensing and meteorological station monitoring, utilizing Moderate Resolution Imaging Spectroradiometer (MODIS), Cloud-Aerosol Lidar and Infrared Pathfinder Satellite Observations (CALIPSO), and the Aerosol Robotic Network (AERONET) to analyze the three-dimensional distribution of aerosol [22,23]. Additionally, meteorological reanalysis data and the Hybrid Single-Particle Lagrangian Integrated Trajectory (HYSPLIT) model have been widely used to further investigate the sources and transport pathways of aerosols [24–26]. Chen et al. developed high-resolution monthly AOD datasets for northwestern China and found that aerosols exhibited pronounced seasonal variations, with AOD peaking in spring and reaching a minimum in autumn [27]. Ge et al. employed

the HYSPLIT model to investigate the potential transport characteristics of dust and saline particles in the Ebinur Lake region of northern Xinjiang, revealing significant seasonal and altitudinal differences in the potential dust transport pathways [28].

Numerous studies have examined the spatial distribution and transport pathways of aerosols in Xinjiang, providing valuable insights into the sources and migration mechanisms of regional pollutants. However, most of these studies have primarily focused on individual years or short-term typical events, with relatively limited temporal coverage, making it difficult to comprehensively capture the long-term evolution and seasonal variation patterns of aerosols in the region. Conducting aerosol evolution studies over a longer time series is essential for gaining deeper insights into the characteristics of atmospheric environmental changes and their driving mechanisms in the region. Therefore, this study focuses on Xinjiang as the research area and systematically analyzes the spatiotemporal distribution characteristics and transport processes of regional aerosols by integrating satellite remote sensing data and reanalysis datasets. The objective is to uncover the source characteristics and transport pathways of aerosols across different seasons and subregions of Xinjiang. This research contributes to a more comprehensive understanding of aerosol transport mechanisms in the region and provides scientific support for regional air quality assessment and pollution control.

2. Materials and Methods

2.1. Study Area

Xinjiang, located in northwestern China, features a complex and diverse topography with substantial elevation differences. Its terrain is characterized by the "Three Mountains and Two Basins" pattern: the Altai Mountains in the north, the Kunlun Mountains in the south, and the Tianshan Mountains running through the central part of the region. The Tianshan Mountains serve as a natural divide, separating Xinjiang into Northern Xinjiang (NXJ) and Southern Xinjiang (SXJ) (Figure 1). The Junggar Basin is the main lowland in Northern Xinjiang, with an elevation ranging from 200 to 1000 m. Southern Xinjiang is centered around the Taklamakan Desert, the second largest shifting sand desert in the world, with elevations between 800 and 1300 m. This region has a strong dust source and frequent aerosol activity [29–31]. Representative cities such as Urumqi in Northern Xinjiang and Kashgar in Southern Xinjiang exemplify industrial and desert-edge urban types, respectively. Influenced by the combined effects of topography, climate, and atmospheric circulation, these regions exhibit marked differences in aerosol source composition, spatiotemporal distribution, and transport pathways [32].

2.2. Datasets and Products

The datasets and products used in this study are briefly summarized in the table below (Table 1). The specific applications of each dataset are further described in the following sections.

Table 1. Summary of datasets and products used in this study.

Dataset Name	Data Type	Spatial Resolution	Main Parameters/Usage
MCD19A2	Remote sensing product	1 km	AOD (550 nm)
CALIPSO Level 1B/VFM	Remote sensing product	Horizontal: 333 m, Vertical: 30–300 m	532 nm backscatter/Aerosol vertical distribution, type identification

Table 1. *Cont.*

Dataset Name	Data Type	Spatial Resolution	Main Parameters/Usage
MERRA-2	Reanalysis data	0.625° × 0.5°	Aerosol column mass density
ERA5	Reanalysis data	0.25° × 0.25°	Wind fields, geopotential height
CHAP	Integrated product	1 km	$PM_{2.5}$, PM_{10}
GDAS1	Trajectory model input	1° × 1°	Trajectory analysis driver

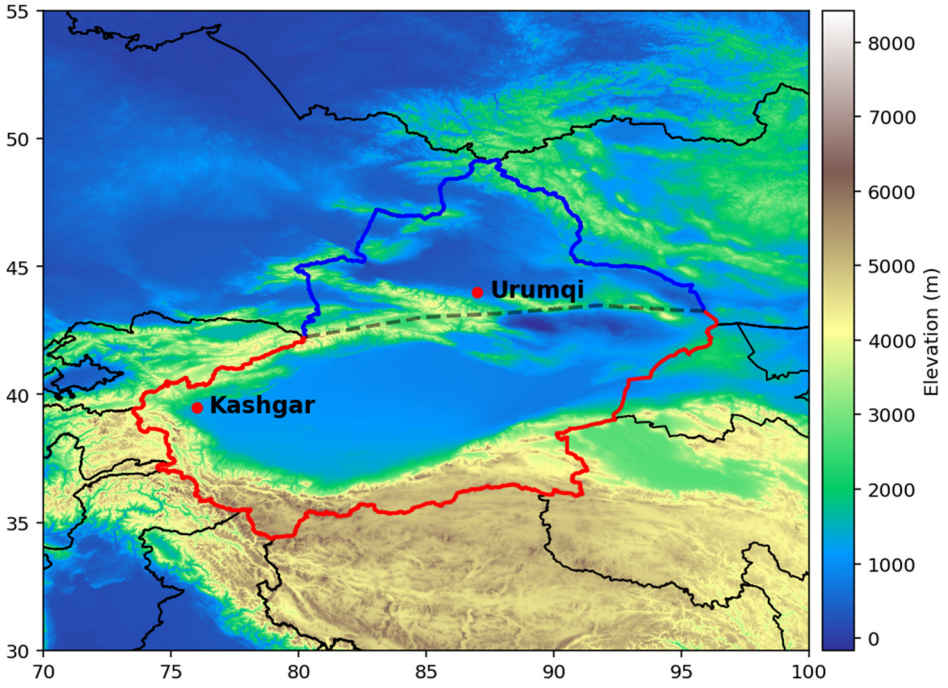


Figure 1. Topographic map of Xinjiang. The gray dashed line in the figure indicates the boundary between northern and southern Xinjiang. The area between this line and the blue solid line represents NXJ, while the area between the dashed line and the red solid line represents SXJ.

2.2.1. MODIS Data

MCD19A2 is an AOD product derived from MODIS observations using the Multi-Angle Implementation of Atmospheric Correction (MAIAC) algorithm. The MAIAC algorithm enhances the accuracy of cloud detection, aerosol retrieval, and atmospheric correction by applying time-series analysis that integrates both pixel-level and image-level processing approaches [33]. The MCD19A2 product provides AOD data at 470 nm and 550 nm wavelengths, along with corresponding quality assurance information (AOD_QA). Previous studies [34,35] have demonstrated that MAIAC AOD performs well in the Central Asian region, including Xinjiang, showing strong agreement with ground-based AOD measurements. Compared to the traditional MYD04 Deep Blue (DB) product, MAIAC offers a greater volume of high-quality retrievals and improved accuracy across various evaluation metrics, effectively addressing the lack of ground-based observation data in the region. In this study, AOD data from the 550 nm band of MCD19A2 are used, with high-quality data selected based on the AOD_QA band. The dataset spans from 1 January 2005 to 31 December 2023. Seasonal definitions are as follows: spring (March–May, MAM), summer (June–August, JJA), autumn (September–November, SON), and winter (December–February, DJF, of the following year).

2.2.2. CALIPSO Profiles

The CALIPSO mission, jointly developed by the National Aeronautics and Space Administration (NASA) and the French National Centre for Space Studies (CNES), was launched on 28 April 2006. Operating in a near-polar sun-synchronous orbit, CALIPSO is designed to monitor atmospheric clouds and aerosols. The satellite is equipped with the Cloud-Aerosol Lidar with Orthogonal Polarization (CALIOP), a dual-wavelength polarization lidar that provides key atmospheric parameters such as backscatter coefficients at 532 nm and 1064 nm, both during daytime and nighttime [36]. In this study, we utilized CALIPSO Level 1B data and the Vertical Feature Mask (VFM) product to extract backscatter profiles and identify and classify aerosol and cloud layers. These datasets enable a detailed examination of the vertical distribution and composition of aerosols, providing insights into their spatial variability in the vertical column. To improve data accuracy and reduce the influence of solar interference, only nighttime observations were utilized in this study.

2.2.3. MERRA-2 Data

The Modern-Era Retrospective analysis for Research and Applications, Version 2 (MERRA-2), developed by the Global Modeling and Assimilation Office (GMAO) at NASA's Goddard Space Flight Center (NASA/GSFC), is the second-generation reanalysis dataset from the MERRA project [37]. In this study, the hourly diagnostic product M2T1NXAER (also referred to as tavg1_2d_aer_Nx) from MERRA-2 was employed to investigate the spatiotemporal variations of different aerosol components over the Xinjiang region. Specifically, we used column mass density variables provided in this dataset—DUCMASS (dust), BCCMASS (black carbon), OCCMASS (organic carbon), and SO4CMASS (sulfate)—to represent different aerosol types, which are predefined by the MERRA-2 system based on the GOCART aerosol module.

2.2.4. ECMWF Data

The meteorological data used in this study were obtained from the fifth-generation reanalysis dataset, ERA5, provided by the European Centre for Medium-Range Weather Forecasts (ECMWF). ERA5 is currently one of the most accurate global reanalysis products, offering a spatial resolution of $0.25^\circ \times 0.25^\circ$ and an hourly temporal resolution. It assimilates a wide range of ground-based and satellite observations using an advanced four-dimensional variational data assimilation system (4D-Var), and has been widely applied in climate and atmospheric environmental studies [38]. In this study, wind fields (U and V components) and geopotential height at 850 hPa and 500 hPa were extracted from ERA5 to analyze the mid- and lower-tropospheric circulation characteristics and aerosol transport pathways over the Xinjiang region.

2.2.5. CHAP Data

The China High-Resolution Air Pollution Dataset (CHAP) is a high-resolution dataset developed for studying air quality and pollutant distributions across China. In this study, CHAP-provided $PM_{2.5}$ and PM_{10} concentration data were used [39,40]. The dataset employs artificial intelligence techniques to fill spatial gaps in satellite-derived MODIS MAIAC AOD data by integrating model simulations, ground-based observations, atmospheric reanalysis data, and emission inventories. As a result, it produces seamless surface pollutant concentration data across China from 2000 to 2023. The accuracy and reliability of CHAP have been rigorously validated by multiple studies, making it a valuable resource for air pollution research.

2.3. Methods

2.3.1. Sen's Slope and Mann–Kendall Test

Sen's slope is a widely used non-parametric method for estimating the linear trend in a time series. It allows for the estimation of the rate of change without relying on assumptions about the data distribution. The calculation formula is as follows:

$$Q = median\left(\frac{x_j - x_i}{j - i}\right),\ 1 \le i \le j \le n \tag{1}$$

The Mann–Kendall (MK) test is a non-parametric statistical method widely used for detecting the significance of trends in time series, particularly in environmental and meteorological studies. Its advantages include independence from the data distribution, robustness to missing values and outliers, and suitability for identifying non-linear trends. The core test statistic is as follows:

$$S = \sum_{i=1}^{n-1} \sum_{j=i+1}^{n} sgn(x_j - x_i) \tag{2}$$

where the sign function, sgn, is defined as follows:

$$sgn(x_j - x_i) = \begin{cases} 1, & x_j - x_i > 0 \\ 0, & x_j - x_i = 0 \\ -1, & x_j - x_i < 0 \end{cases} \tag{3}$$

When the sample size $n > 8$, the normal distribution approximation can be applied, and the test statistic Z is given by:

$$Z = \begin{cases} \frac{S-1}{\sqrt{Var(S)}}, & S > 0 \\ 0, & S = 0 \\ \frac{S+1}{\sqrt{Var(S)}}, & S < 0 \end{cases} \tag{4}$$

At a significance level of $\alpha = 0.05$, a trend is considered statistically significant when the absolute value of the test statistic satisfies $|Z| > 1.96$. To facilitate the interpretation of the trend analysis results, the combined use of Sen's slope and the Mann–Kendall Z statistic is categorized, as shown in Table 2.

Table 2. Trend classification based on Sen's slope and MK Z-statistic.

Criteria	Trend Features
$Q > 0$ and $Z > 1.96$	Significant increasing trend
$Q < 0$ and $Z < -1.96$	Significant decreasing trend
All other cases	Non-significant or inconsistent trend

2.3.2. Backward Trajectory Analysis

In this study, the MeteoInfo software (v3.9.11) was employed to visualize atmospheric trajectories and identify potential aerosol source regions. MeteoInfo is a visualization and analysis platform that integrates Geographic Information System (GIS) capabilities and supports trajectory simulation, statistical analysis, and spatial data visualization [41]. The trajectory simulations were based on the Hybrid Single-Particle Lagrangian Integrated Trajectory (HYSPLIT) model [42], developed by the National Oceanic and Atmospheric Administration (NOAA), which has been widely used for tracking air mass transport and identifying pollution sources. The meteorological input for HYSPLIT was obtained from

NOAA's Global Data Assimilation System (GDAS), accessible via https://ready.arl.noaa.gov/index.php (accessed on 24 April 2025). In this study, the backward trajectories were computed with a temporal resolution of 6 h, a duration of 48 h, and starting altitudes above ground level of 0.5 km and 1.5 km to analyze aerosol transport characteristics at different atmospheric levels. However, since backward trajectories track the movement of air masses rather than pollutants in the atmosphere, they cannot identify the relative contribution of different assumed source regions to air pollution in the study area. To further analyze the potential source regions of pollutants, the Concentration Weighted Trajectory (CWT) method was subsequently employed [43,44].

CWT is a trajectory-based source apportionment method used to identify potential source regions contributing to regional pollution. This method combines air mass trajectories with ground-based pollutant concentration data, calculating the average pollutant concentration associated with each air mass at every grid cell. It quantifies the potential contribution of each region to the pollution levels at the receptor point. The calculation method is as follows:

The study region is divided into a grid of $i \times j$ cells. For each grid cell (i, j), the CWT calculation formula is as follows:

$$CWT_{ij} = \frac{\sum_{k=1}^{N} C_k \cdot \tau_{ijk}}{\sum_{k=1}^{N} \tau_{ijk}} \tag{5}$$

where C_k represents the pollutant concentration associated with the k-th trajectory, τ_{ijk} denotes the residence time of the k-th trajectory within grid cell (i, j), and N is the total number of trajectories. To reduce the uncertainty in regions with low trajectory frequency, a weight function is typically introduced to adjust the CWT values, resulting in the Weighted Concentration Weighted Trajectory (WCWT) method [45]. The core concept of WCWT is to assign lower confidence to grid cells with fewer trajectories, thereby downscaling their potential impact on the receptor site. A commonly used weighting function is defined as:

$$W_{ij} = \begin{cases} 1.0, n_{ij} > 3n_{avg} \\ 0.7, 1.5n_{avg} < n_{ij} \leq 3n_{avg} \\ 0.42, n_{avg} < n_{ij} \leq 1.5n_{avg} \\ 0.05, n_{ij} \leq n_{avg} \end{cases} \tag{6}$$

where W_{ij} is the weight for grid cell (i, j), n_{ij} denotes the number of trajectories passing through grid cell (i, j), and n_{avg} represents the average number of trajectories across all grid cells. The final form of the WCWT is then given by:

$$WCWT_{ij} = W_{ij} \cdot CWT_{ij} \tag{7}$$

3. Results

3.1. Spatiotemporal Characteristics of Aerosols over Xinjiang

3.1.1. The Spatiotemporal Variation Characteristics of AOD

Figure 2 illustrates the spatial distribution characteristics of AOD across Xinjiang during each season from 2005 to 2023. Overall, a clear distinction in AOD levels between southern and northern Xinjiang is observed, with SXJ generally exhibiting higher AOD values than NXJ. In SXJ, higher AOD values are primarily concentrated in the Taklamakan Desert and surrounding areas, while in NXJ, high AOD values are mainly found around the cities located to the north of the Tianshan Mountains. During spring, SXJ experiences the highest AOD, with an average value reaching 0.8, while AOD decreases sequentially

through summer, autumn, and winter, with winter averaging only about 0.25. Notably, during winter, the AOD levels in NXJ are comparable to those in SXJ. Figure 3 shows the interannual variability of AOD in both SXJ and NXJ from 2005 to 2023. Although seasonal and regional differences exist, the overall annual mean AOD across Xinjiang has not shown a distinct monotonic increase or decrease over the past two decades. Spring in SXJ consistently exhibits the highest AOD with considerable interannual fluctuation, while AOD in NXJ shows a more stable seasonal variation, fluctuating between 0 and 0.2, with relatively higher values observed in winter.

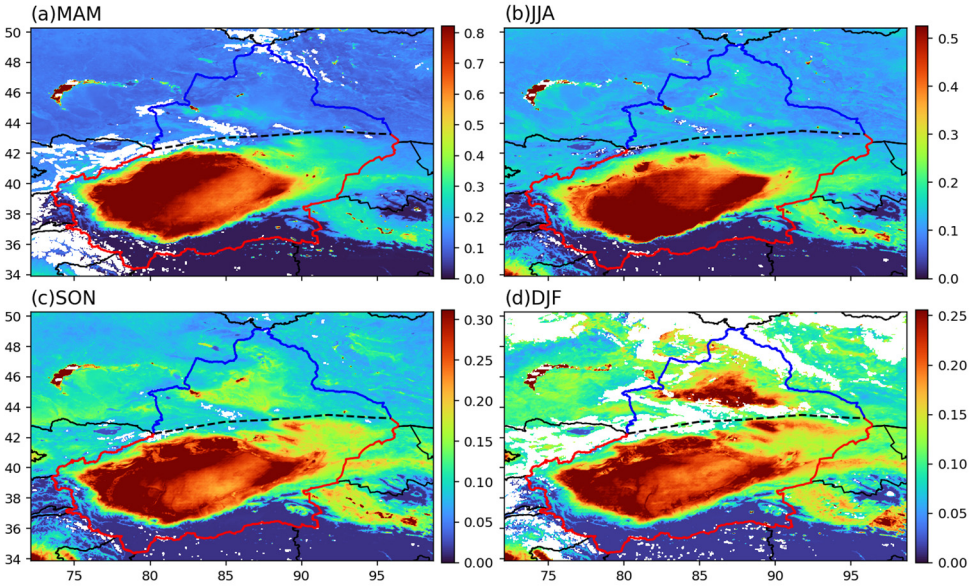


Figure 2. The spatial distribution of the mean AOD values in Xinjiang for the four seasons from 2005 to 2023.

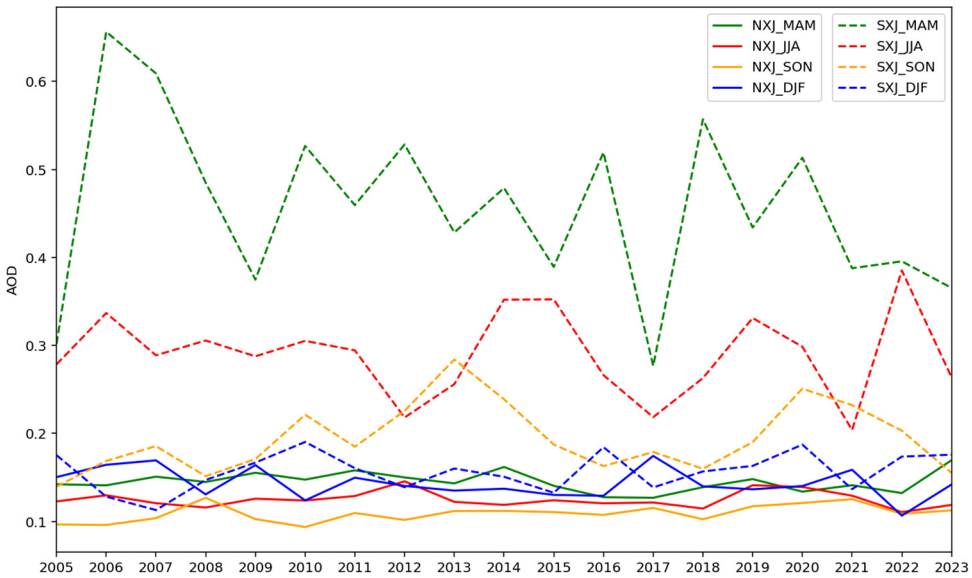


Figure 3. The AOD time series of the four seasons in southern and northern Xinjiang from 2005 to 2023.

Trend analysis using Sen's slope estimation and the Mann–Kendall test was performed to assess the significance and direction of seasonal changes. As the results were largely non-significant, they are summarized in the Supplementary Materials Figure S1.

3.1.2. The Spatial Distribution and Differences in Aerosol Components

Xinjiang, located in the heart of the Eurasian continent, is characterized by its arid climate, strong winds, and the presence of the Taklamakan Desert, making dust aerosols (DU) the predominant atmospheric aerosol type in the region [46]. Moreover, the exploitation and utilization of resources such as coal and oil release significant quantities of anthropogenic aerosol components, such as organic carbon (OC), black carbon (BC), and sulfate aerosols (SO4). Under specific meteorological conditions, these anthropogenic aerosols can mix with natural dust particles, forming polluted dust with enhanced hygroscopicity and radiative effects [47].

Figure 4 illustrates the spatial distribution of column mass density for major aerosol components across Xinjiang. Dust aerosols show marked spatial variation between southern and northern regions. High concentrations are primarily located in desert areas, with the Taklamakan Desert being the most prominent, followed by the Gurbantünggüt Desert in the north. In contrast, anthropogenic aerosols such as sulfates, black carbon, and organic carbon exhibit a more uniform distribution, with elevated levels near urban and industrialized areas. Dust aerosols exhibit substantially higher column mass densities than other aerosol types, followed by sulfates, organic carbon, and black carbon. Figure 5 presents the seasonal variation in the column mass density of major aerosol components across Xinjiang. In NXJ, dust aerosols account for 94.13% of the total column mass, while in SXJ, the proportion increases to 97.77%. In the north, dust aerosol levels exhibit a clear seasonal decline from spring to winter. In contrast, in the south, dust concentrations remain relatively high during summer, whereas the north sees a noticeable drop in the same period. This contrasting pattern may be attributed to regional differences in precipitation, as increased summer rainfall in the north likely enhances the wet deposition of dust aerosols [48]. Meanwhile, sulfates, organic carbon, and black carbon show minimal seasonal variation, with relatively minor differences between the two subregions.

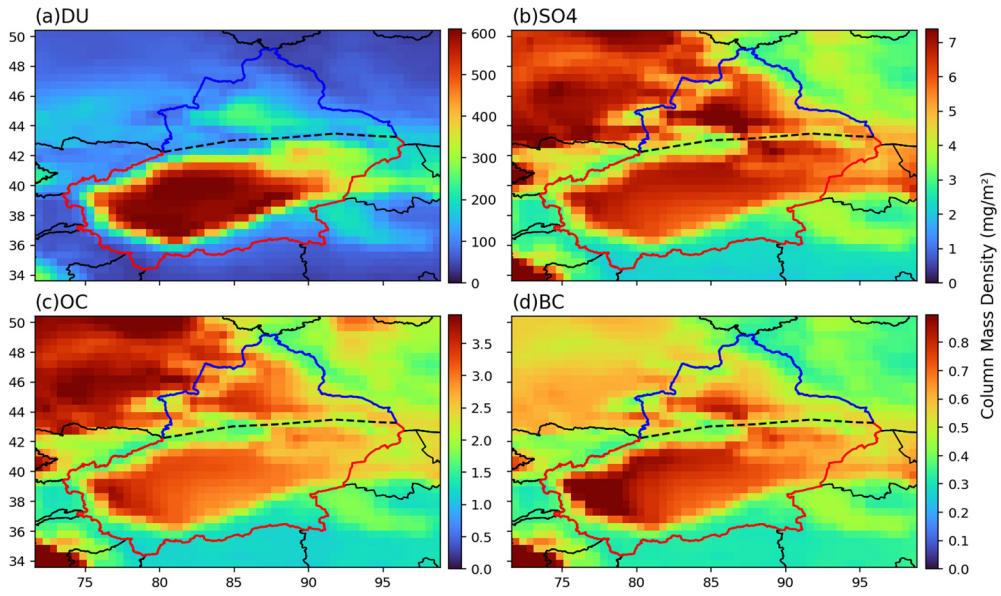


Figure 4. Spatial distribution of column mass density of the main aerosol components in Xinjiang.

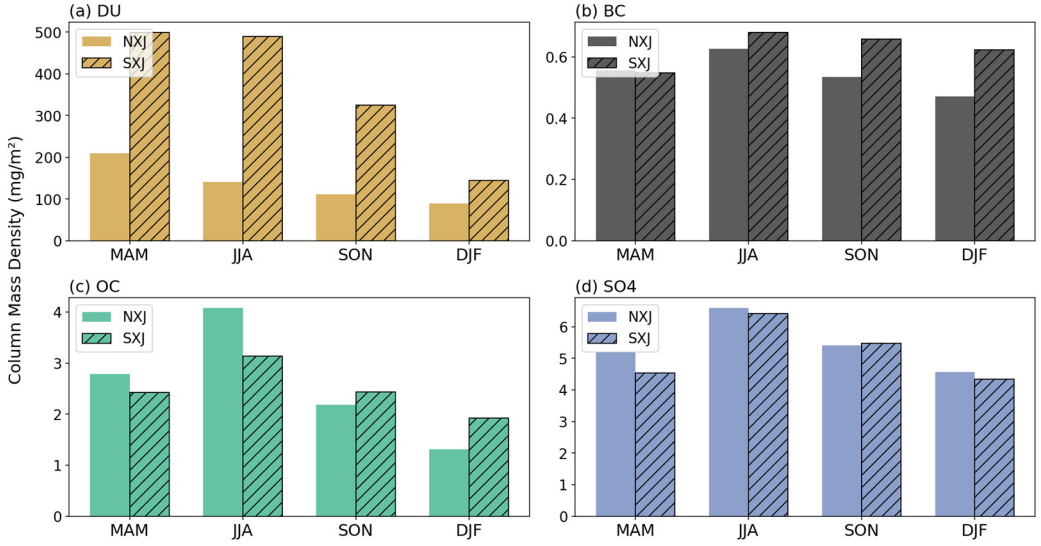


Figure 5. Seasonal column mass density of major aerosol components in Xinjiang.

3.1.3. The Spatiotemporal Variation Characteristics of $PM_{2.5}$ and PM_{10}

$PM_{2.5}$ and PM_{10} are commonly used indicators of ground-level aerosol mass concentrations and effectively reflect variations in near-surface aerosol levels. To a certain extent, they serve as representative parameters for assessing changes in surface aerosol loading and are widely applied in air quality evaluations as well as comparative analyses with satellite-derived retrievals [49]. The spatial distribution characteristics of $PM_{2.5}$ and PM_{10} closely resemble those of AOD (Figure S2 in the Supplementary Materials). During spring, summer, and autumn, $PM_{2.5}$ concentrations in SXJ remain consistently high. In winter, however, a notable increase in $PM_{2.5}$ is observed in NXJ, particularly in urban areas such as Urumqi, while the overall concentrations in SXJ are relatively low, with elevated values only in localized areas such as the western Taklamakan Desert and the city of Kashgar. In contrast, PM_{10} concentrations in SXJ are generally high throughout all seasons, and in winter, elevated PM_{10} levels are also observed in northern cities including Urumqi.

To more intuitively reveal the long-term aerosol evolution in key regions of Xinjiang, Urumqi and Kashgar were selected as representative cities of northern and southern Xinjiang, respectively. Both cities exhibit distinct seasonal variations, with elevated levels primarily in spring and winter, while long-term trends remain ambiguous (Figure S3 in the Supplementary Materials). Notable differences are observed between the two cities: Kashgar consistently records higher concentrations of both $PM_{2.5}$ and PM_{10} compared to Urumqi. Specifically, the annual mean concentrations of $PM_{2.5}$ and PM_{10} in Kashgar reach 96.78 $\mu g/m^3$ and 276.22 $\mu g/m^3$, respectively, substantially exceeding those in Urumqi, which are 57.23 $\mu g/m^3$ and 117.56 $\mu g/m^3$.

3.2. Characteristics of Aerosol Transport in Typical Spring and Winter in Xinjiang

This study focuses on spring and winter, the seasons exhibiting the most pronounced spatiotemporal variations in aerosol distribution. Taking the year 2022 as a representative case, an in-depth analysis is conducted from the perspectives of aerosol vertical distribution characteristics, meteorological drivers, and backward trajectory and source region identification, in order to elucidate the seasonal differences in aerosol transport pathways and source structures between southern and northern Xinjiang.

In 2022, the temporal trends of $PM_{2.5}$ and PM_{10} concentrations in Urumqi and Kashgar were generally consistent; however, Urumqi showed more distinct seasonal variations (Figure 6). In Urumqi, both $PM_{2.5}$ and PM_{10} concentrations peaked during winter and gradually declined in spring. Concurrently, the $PM_{2.5}/PM_{10}$ ratio also decreased, indi-

cating a relative reduction in the proportion of fine particles. Starting in November, both concentrations and their ratio began to rise again, suggesting a transitional shift in pollution characteristics from autumn to winter. In contrast, aerosol concentrations in Kashgar remained relatively stable, though the $PM_{2.5}/PM_{10}$ ratio also showed a downward trend from winter to spring before stabilizing. Notably, Kashgar exhibited several prominent concentration peaks not only in spring and winter but also during summer and autumn, highlighting a more complex seasonal profile of aerosol pollution in SXJ.

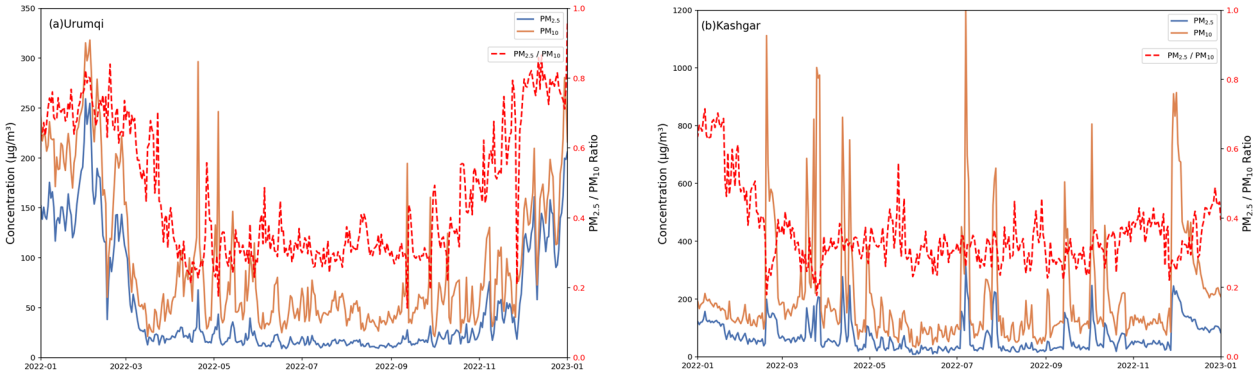


Figure 6. Time series of $PM_{2.5}$, PM_{10}, and $PM_{2.5}/PM_{10}$ Ratio in Urumqi and Kashgar (2022).

In order to study the vertical distribution characteristics of aerosols in Xinjiang during spring and winter, the backscattering coefficients and vertical characteristic mask products of CALIPSO on 5 February and 4 April 2022 were analyzed. As can be seen from Figure 7, the aerosols on 5 February were mainly distributed near the ground, highly concentrated below 5 km. Aerosol types include both dust aerosols and polluting dust components. Compared with the CALIPSO backscattering profile in February, the profile on 4 April shows a significantly enhanced backscattering signal in the 5–12 km upper layer, indicating an increase in aerosol concentration within this height range. Combined with the VFM data, it can be seen that aerosols are widely distributed within this height range, indicating that these aerosols may originate from the high-altitude transportation process. Such phenomena are usually closely related to the vertical atmospheric transport mechanism, especially in spring, when strong winds and unstable atmospheric clots facilitate the lifting and long-distance transport of ground dust and polluting aerosols. The SXJ and NXJ regions show relatively consistent characteristics in terms of aerosol types, mainly consisting of sand and dust aerosols, accompanied by a small amount of pollution-type aerosols. In spring, sand and dust activities are frequent. Under the influence of strong winds, deserts and arid areas are prone to generating a large amount of sand and dust aerosols. At the same time, pollutants produced by human activities may also be mixed in, forming aerosol components with certain complexity.

Further analysis, combined with wind vector and geopotential height maps at the time of the satellite overpasses (Figure S4 in the Supplementary Materials), reveals that on 5 February, at the 500 hPa level, a distinct geopotential height low-value center was observed over western Xinjiang, indicating the influence of a mid- to upper-level low-pressure system. Under the influence of this system, southeastern winds in NXJ, however, the low wind speeds were not conducive to horizontal aerosol transport, resulting in the accumulation of pollutants near the surface. In contrast, SXJ experienced stronger northwesterly winds, suggesting a certain potential for horizontal transport. However, the absence of significant upper-level aerosol activity in the CALIPSO observations indicates that the wind field had not yet triggered significant high-altitude transport processes.

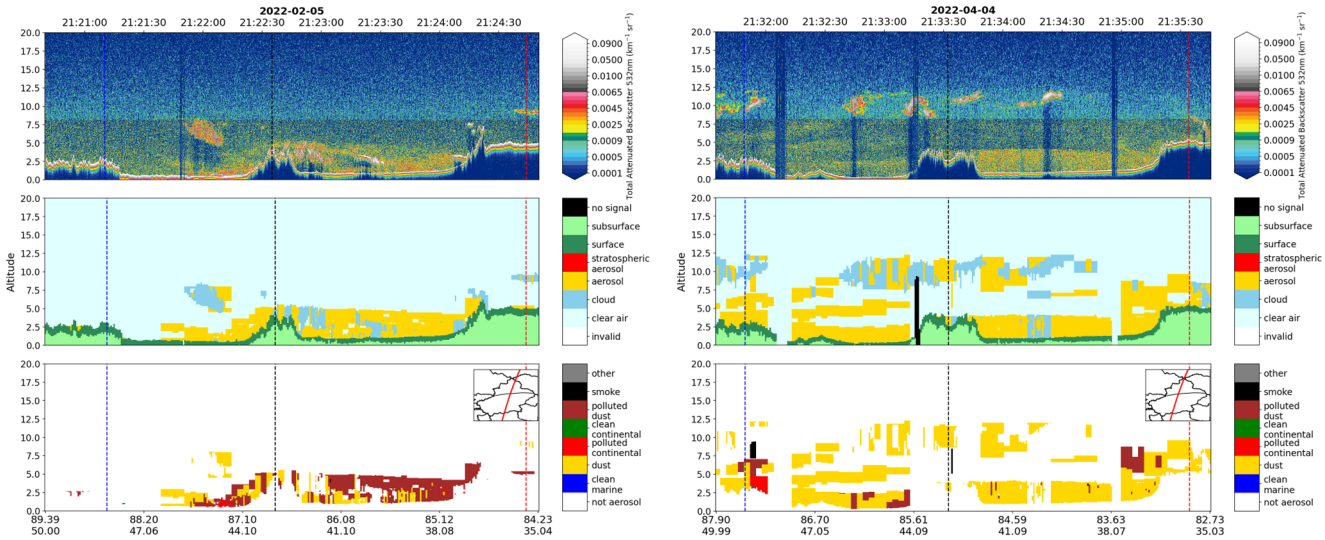


Figure 7. CALIPSO 532 nm total attenuation backscattering coefficient, vertical characteristic mask, and aerosol type (UTC) for 5 February 2022 (**left**) and 4 April 2022 (**right**). The blue, black, and red dashed lines represent the intersections of the satellite trajectory with the northern boundary of NXJ, the boundary between northern and southern Xinjiang, and the southern boundary of SXJ, respectively.

At the 850 hPa level, a geopotential height low-value center was still present in the northwestern part of Xinjiang, while a high-value center appeared in the northeastern region, possibly influenced by the terrain. This led to a highly uneven wind vector field: in NXJ, wind speeds were high, but the wind directions were chaotic, indicating frequent lower-level disturbances and a lack of a sustained prevailing wind direction, which is unfavorable for long-range transport. In contrast, SXJ experienced lower wind speeds with similarly disordered wind directions, reflecting a more stable lower atmosphere where uplift and transport processes were limited. Although disturbances existed in both the upper and lower atmosphere, the combined effects of wind speed, wind direction, and vertical dynamics resulted in a localized accumulation of aerosols, with a lack of favorable conditions for large-scale vertical or horizontal transport.

At the 500 hPa level on 4 April, NXJ experienced strong northwesterly winds, with a distinct northwesterly transport channel at higher altitudes, providing favorable conditions for aerosol transport at elevated levels. There was also a transport path extending over the Tianshan Mountains toward SXJ, suggesting the possibility of pollutants from NXJ being transported to SXJ via upper-level winds. At 850 hPa, the lower atmosphere in NXJ was relatively stable with low wind speeds, while in SXJ, the wind directions were more chaotic, indicating local disturbances that caused uneven low-level airflow. Overall, the atmospheric circulation was weak, hindering the diffusion of surface pollutants.

To investigate the origins and transport characteristics of air masses over Urumqi and Kashgar during the spring and winter of 2022, backward trajectory cluster analysis was conducted at two representative altitudes: 500 m and 1500 m above ground level. The potential source regions of air masses were categorized into the following geographic domains: Central Asia (including Turkmenistan, Uzbekistan, Kyrgyzstan, Tajikistan, and Kazakhstan), West Asia (covering Turkey, Iran, Iraq, and 16 additional countries and regions), South Asia (including India, Pakistan, and five other nations), Russia, Mongolia, Europe, and Local. Air masses were classified as "Local" if their trajectory endpoints fell within the boundaries of Xinjiang. To further assess potential interactions or mutual influence between northern and southern Xinjiang, locally sourced air masses were subdivided into NXJ and SXJ based on their trajectory endpoints. This approach allows for a detailed examination of regional transport patterns and the extent to which interregional aerosol exchange occurs within Xinjiang.

Figure 8 presents the backward trajectories of air masses at 500 m and 1500 m over Urumqi and Kashgar during the spring and winter of 2022. In winter, air masses at 500 m over Urumqi were predominantly of local origin, accounting for 68.64% of all trajectories, with the remainder primarily originating from Central Asia. Similarly, in Kashgar, local air masses made up 62.43% of the total, while the rest mainly came from northern West Asia. At the 1500 m level, air masses exhibited longer transport distances. The proportion of locally sourced trajectories over Urumqi decreased to 38.33%, with the remaining three trajectory clusters originating from Central Asia. In Kashgar, the proportion of local air masses further dropped to 29.01%, with the rest sourced from northern West Asia and southern Central Asia.

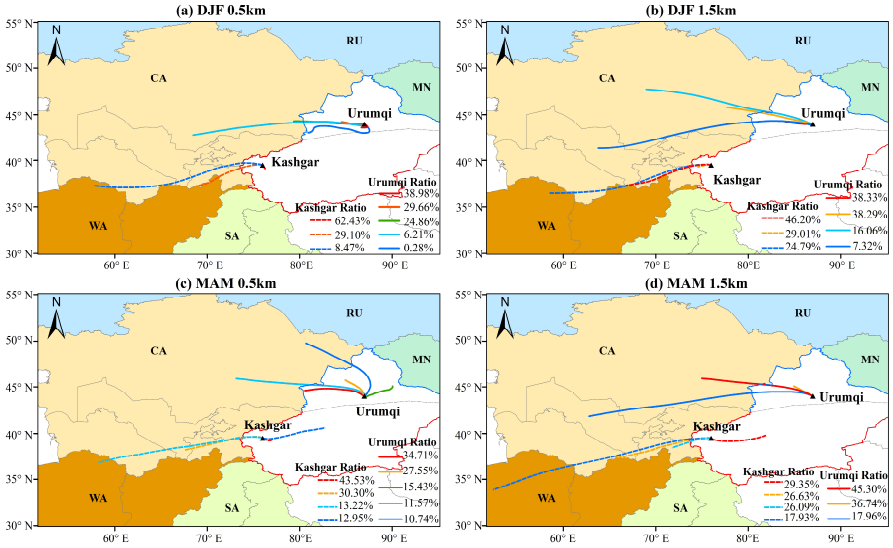


Figure 8. Backward trajectories of air masses for Urumqi and Kashgar in 2022.

During spring, 500 m air masses over Urumqi were again dominated by local sources (77.69%), with the rest coming from eastern Central Asia. In Kashgar, 56.48% of the air masses were local, while 12.95% were traced to the Taklamakan Desert—an origin not observed in winter—and the remainder were from northern West Asia and southern Central Asia. At 1500 m altitude in spring, the air mass transport range expanded. Over Urumqi, the proportion of local trajectories dropped to 36.74%, with the remainder mainly from Central Asia. In Kashgar, only one trajectory cluster was of local origin (29.35%), while the others originated from West Asia, northern Central Asia, and regions in Central Asia adjacent to Kashgar. Overall, the analysis indicates that lower-altitude air masses (500 m) in both spring and winter exhibit strong local characteristics, whereas higher-altitude air masses (1500 m) are more significantly influenced by long-range transport.

In conjunction with ground-based $PM_{2.5}$ observations, the CWT method was employed to further identify potential source regions and assess the seasonal and vertical variations in air mass influence on regional pollution (Figure 9). At 500 m during winter, high CWT values over Urumqi were primarily concentrated in the urban periphery, indicating that local emissions were the dominant source of pollution, with limited contribution from regional transport. In contrast, Kashgar exhibited not only local high-value zones but also significant CWT values over parts of West Asia, suggesting a notable influence from long-range transported pollutants during the winter season.

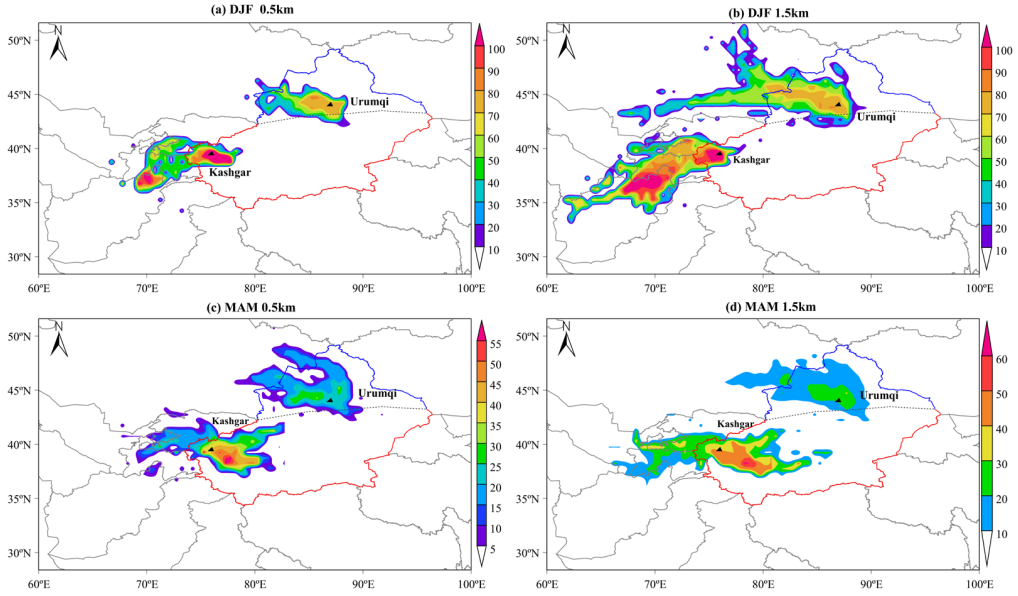


Figure 9. Spatial distribution of CWT for Urumqi and Kashgar in 2022.

At 1500 m during winter, the spatial extent of high CWT values broadened. Potential source regions for Urumqi extended westward into Central Asia, indicating an increased contribution from long-range upper-air transport. Similarly, high CWT zones over Kashgar expanded southwestward, suggesting a greater influence of transboundary pollution at higher altitudes.

During spring, overall CWT values were lower than in winter, indicating a reduced level of regional pollution. In Urumqi, high-value areas became more spatially concentrated, suggesting a more localized impact from pollution sources. In contrast, Kashgar showed an emerging trend of potential sources expanding toward the Taklamakan Desert, particularly at the 1500 m level, where the influence of elevated layers became more pronounced. These results highlight distinct seasonal and vertical differences in the spatial patterns of potential aerosol source regions, emphasizing the stronger role of long-range transport in winter and at higher altitudes, especially for SXJ.

To further explore the long-term evolution of aerosol transport over Xinjiang, a systematic analysis of air mass trajectories and source region distributions from 2005 to 2023 was conducted (Figures 10 and 11). During winter, air masses arriving in Urumqi predominantly originated from local and Central Asian regions, with fewer trajectories traced to Russia and SXJ. Notably, no air masses originated from local sources in 2008 and 2009; in 2008, a small number were traced to SXJ, whereas in 2009, all trajectories originated from Central Asia. Overall, the distribution of source regions showed no significant interannual variation. At 1500 m, the origin characteristics of air masses changed markedly: the proportion of locally sourced air masses decreased significantly, while those from Central Asia increased. In spring, compared with winter, the share of local air masses further declined, and trajectories at 1500 m showed expanded source regions, including Mongolia and Europe. Overall, with increasing altitude, the contribution from local sources diminished, whereas the influence of long-range transport became more prominent. The analysis of air mass origins over Kashgar during winter indicates that they primarily originated from local regions, Central Asia, and West Asia. At 500 m, the proportion of locally sourced air masses remained low before 2010, but increased significantly thereafter, accompanied by a rise in the contribution from West Asia. At 1500 m, air masses from South Asia appeared among the source regions, while those from West Asia became dominant and the share of local air masses declined. During spring, Kashgar's air masses were mainly sourced from local areas and Central

Asia, with a reduced proportion from West Asia. Similar to the pattern observed in Urumqi, an increase in trajectory altitude led to a lower contribution from local sources.

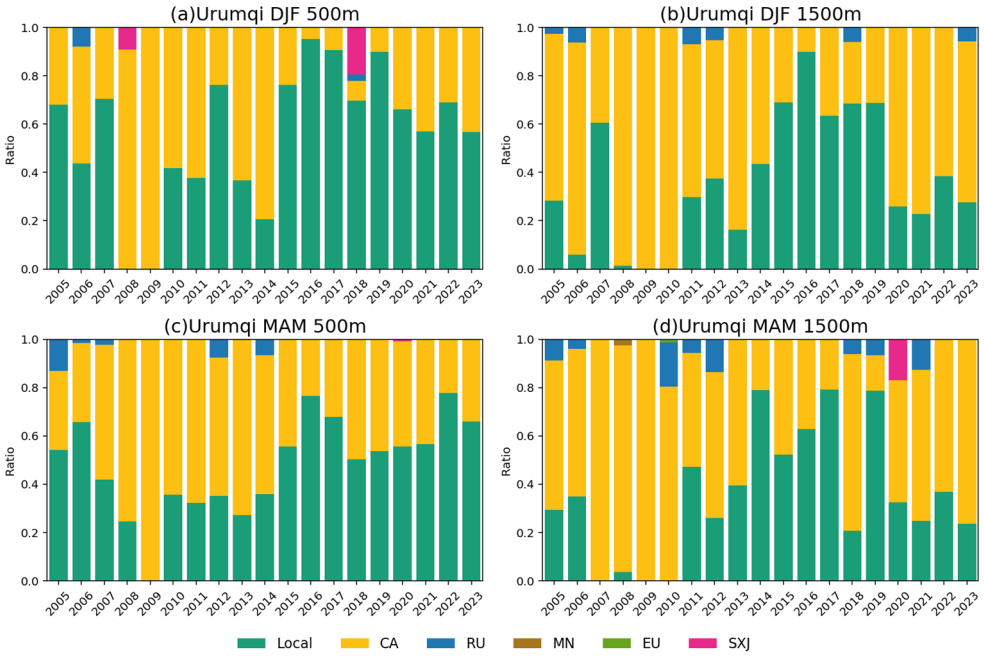


Figure 10. The source of backward trajectories of air masses in Urumqi from 2005 to 2023.

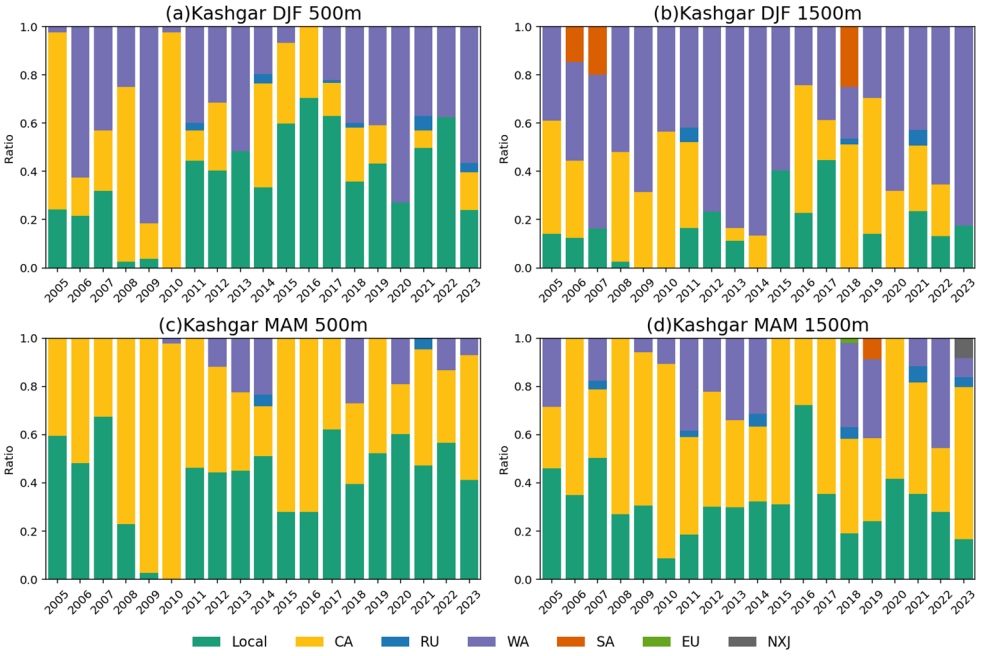


Figure 11. The source of backward trajectories of air masses in Kashgar from 2005 to 2023.

Figures 12 and 13 depict the spatial distribution of CWT values at 500 m and 1500 m above ground level over Urumqi and Kashgar during spring and winter from 2005 to 2023. The spatial and temporal patterns presented are generally consistent with those observed in Figure 9. In winter, potential pollution sources in Urumqi are primarily confined to the local area, highlighting the dominant role of local emissions in regional air pollution. However, at 1500 m above ground level, the source regions extend into Central and Western Asia, indicating a greater contribution from long-range transport at higher altitudes. In spring, the spatial distribution of source regions becomes more dispersed, although local sources still prevail overall. This pattern suggests that regional

atmospheric circulation exerts a stronger influence in spring, leading to more complex pollutant transport pathways. Notably, the extension of source regions across the Tianshan Mountains to the southern slopes implies that pollutants from SXJ may be transported northward across the mountain barrier. In Kashgar, winter pollution sources are primarily concentrated locally and over southern Central Asia and northern Western Asia, with a pronounced southwestward extension. This distribution may be attributed to low wind speeds and stable meteorological conditions during winter, which suppress the northward transport of dust from the Taklimakan Desert. In contrast, during spring, elevated CWT values are prominently centered over the Taklimakan Desert, indicating that dust transport becomes a key driver of regional air pollution. Moreover, at the 1500 m level, potential source regions extend northward toward NXJ, possibly due to springtime meteorological conditions that facilitate southward pollutant transport through lower-altitude mountain passes or valleys in the eastern Tianshan range.

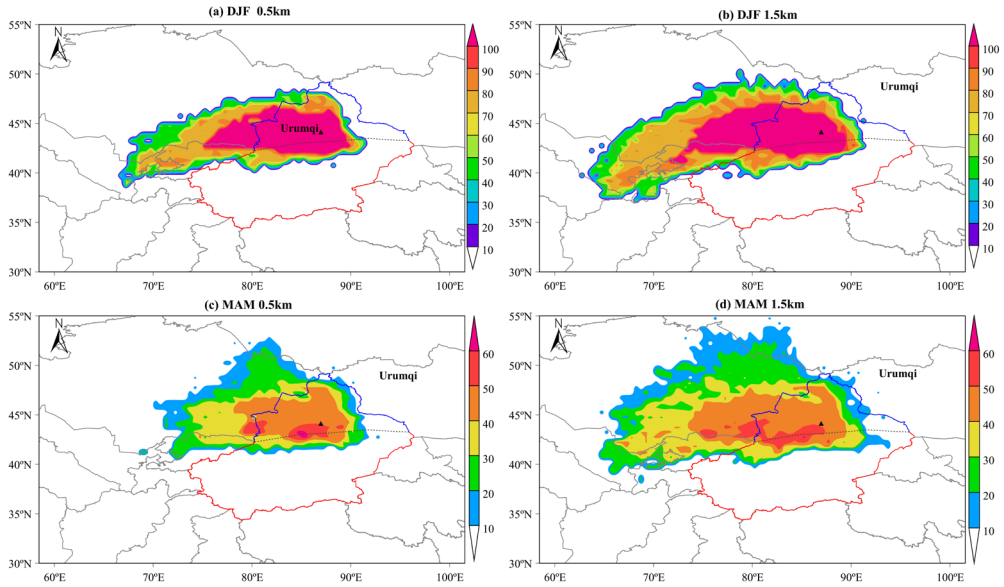


Figure 12. Spatial distribution of CWT in Urumqi from 2005 to 2023.

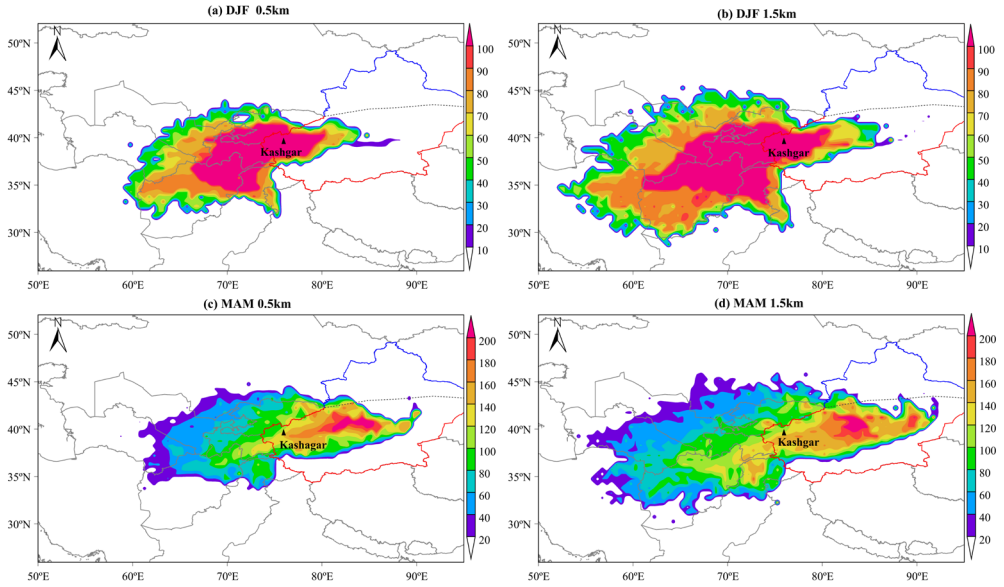


Figure 13. Spatial distribution of CWT in Kashgar from 2005 to 2023.

4. Discussion

This study first employed high-resolution MCD19A2 AOD data, in conjunction with MERRA-2 aerosol reanalysis, to examine spatial differences in AOD across Xinjiang from 2005 to 2023, focusing on regional and seasonal variations as well as dominant aerosol types. In addition, the Chinese high-resolution air quality dataset ($PM_{2.5}$ and $PM_{2.5}$) was used to analyze the distribution of near-surface aerosols and to investigate the temporal trends in $PM_{2.5}$ and PM_{10} concentrations.

The results reveal significant spatial heterogeneity and seasonal variability in aerosols over Xinjiang. AOD levels in SXJ are markedly higher than those in the north, which is unsurprising given the presence of the Taklamakan Desert—a major source of dust in the region. This is particularly evident in spring, when AOD, $PM_{2.5}$, and PM_{10} concentrations in SXJ increase substantially. This phenomenon is likely closely related to the region's unique climatic conditions and complex topography. In spring, SXJ typically experiences arid and rain-scarce conditions. Coupled with the intensified westerlies and strong atmospheric circulation, loose surface materials are more easily lifted into the atmosphere, leading to frequent dust storm events. Additionally, the Tarim Basin, characterized by a typical enclosed topography, hinders both horizontal dispersion and vertical dilution of aerosols. This facilitates the accumulation of dust and other particulates, resulting in high concentrations of aerosol layers in the region [50]. In contrast, NXJ exhibits severe aerosol pollution during winter, which may be closely related to emissions from centralized heating systems [46,51]. The region is often dominated by cold high-pressure systems in winter, accompanied by low temperatures, frequent temperature inversions, and enhanced near-surface atmospheric stability. Furthermore, generally low wind speeds during this season suppress vertical mixing, thereby allowing pollutants to accumulate near the surface and contributing to elevated AOD levels [52].

Dust aerosol is the predominant aerosol type in both southern and northern Xinjiang, with a pronounced seasonal pattern characterized by concentrations highest in spring, followed by summer and autumn, with the lowest in winter [53]. The column mass densities of black carbon, organic carbon, and sulfate aerosols show little difference between the north and south. This is likely due to the relatively weak anthropogenic emission intensity in both regions. Although NXJ has higher levels of urbanization and industrial activity, the small-scale differences in local emissions are not significant at the resolution of the MERRA-2 dataset [54].

To further analyze the sources and transport of aerosols in northern and southern Xinjiang, CALIPSO profile data, ERA5 reanalysis data, and backward trajectory models were utilized. Taking 2022 as a case study, a detailed analysis of the vertical distribution characteristics, meteorological drivers, and sources of aerosols in Urumqi and Kashgar during spring and winter was conducted. The study found that in winter (5 February 2022), aerosols were predominantly deposited at the surface, with short-distance transport primarily occurring at low altitudes. Both northern and southern Xinjiang experienced pollutant-laden dust aerosols, a result of increased anthropogenic aerosol emissions due to heating activities during the winter [55]. Additionally, unfavorable meteorological conditions, such as low temperatures and atmospheric stability, exacerbated the accumulation of pollutants. Moreover, the influence of surrounding deserts led to the presence of natural dust aerosols in the region. The interaction of anthropogenic pollution sources and natural dust sources contributed to the complex aerosol characteristics observed. In contrast, during spring (4 April 2022), a noticeable phenomenon of high-altitude aerosol transport emerged, with a reduction in pollutant-laden dust. Wind direction, wind speed, and atmospheric pressure played a crucial role in aerosol transport [56]. The atmospheric circulation at 500 hPa was relatively stable, with a consistent wind direction and high wind

speeds, which facilitated long-range aerosol transport. In comparison, at lower altitudes (850 hPa), the wind direction was more chaotic with significant local disturbances, making the aerosol transport direction unstable and limiting the transport distance, leading to potential retention and accumulation.

Additionally, aerosol transport is influenced by topography. Both the significant differences in AOD between northern and southern Xinjiang and the backward trajectory analyses for Urumqi and Kashgar demonstrate that the Tianshan Mountains act as a barrier [57], preventing large-scale air mass exchange between the two regions. In Urumqi, air masses primarily originate from local and Central Asia sources, with local pollution dominating in winter, while the monsoon in spring reduces the influence of local pollution. Similarly, in Kashgar, pollution mainly comes from local sources and northern Western Asia. In winter, local contributions dominate, but in spring, the region is more susceptible to pollution from the central part of the Taklamakan Desert. Furthermore, the increase in air mass altitude not only extends the transport distance but also reduces the proportion of local air masses. Considering that extending the backward trajectory simulation time increases the uncertainty of the results, the simulation time in this study was set to 48 h, and therefore no significant long-range transport phenomena were observed.

5. Conclusions

This study systematically investigates the spatiotemporal variation characteristics and potential transport sources of aerosols in Xinjiang from 2005 to 2023, based on remote sensing data, reanalysis datasets, and backward trajectory models. The main conclusions are as follows:

(1) The Aerosol Optical Depth (AOD) in Xinjiang exhibits significant spatiotemporal distribution characteristics. In terms of temporal scale, NXJ shows small seasonal fluctuations, with the peak AOD occurring in winter, while SXJ exhibits clear seasonal variation, with the highest AOD in spring and the lowest in winter, and significant interannual variability. However, no clear upward or downward trend is observed overall. Spatially, the AOD in SXJ is generally higher than in NXJ, with high AOD values primarily found in urban areas of NXJ. Overall, dust aerosols are the dominant aerosol type in Xinjiang.

(2) In winter, aerosols in Xinjiang mainly deposit in the near-surface layer, influenced by local and short-distance transport. In contrast, spring shows a distinct characteristic of high-altitude long-range transport. With increasing air mass height, the contribution of local air masses gradually decreases, and the transport distance significantly increases. Backward trajectory analysis shows that pollution air masses in Urumqi mainly originate from local and Central Asia sources, with higher pollution levels in winter compared to spring. In Kashgar, winter pollution air masses mainly come from local, southern Central Asia, and northern Western Asia sources, while in spring, pollution primarily originates from the Taklamakan Desert, with significantly higher pollution levels than in winter.

This study reveals the spatiotemporal characteristics and transport mechanisms of aerosol variation in Xinjiang, providing scientific references for regional atmospheric environmental management and dust control. Future studies can further deepen the understanding of aerosol sources and evolution processes by combining chemical composition observations and model simulations.

Supplementary Materials: The following supporting information can be downloaded at: https://www.mdpi.com/article/10.3390/rs17132207/s1.

Author Contributions: Conceptualization, C.L. and X.L.; methodology, C.L. and W.L.; investigation, C.L., Z.T., Q.Z. and M.F.; writing—original draft preparation, C.L.; writing—review and editing, C.L. and X.L.; visualization, C.L.; supervision, X.L. All authors have read and agreed to the published version of the manuscript.

Funding: This work was supported in part by the National Natural Science Foundation of China under Grant 42075114, in part by the Priority Academic Program Development of Jiangsu Higher Education Institutions under Grant 140119001, in part by the 2024 Qinghai Province "Kunlun Talents—Leading Talent in Science and Technology" Program (Young Science and Technology Talent Support Initiative).

Data Availability Statement: Publicly available datasets were analyzed in this study. MCD19A2 and CALIPSO aerosol data can be found here: [https://www.earthdata.nasa.gov/ (last accessed on 20 April 2025)]. MERRA-2 data can be found here: [https://gmao.gsfc.nasa.gov/reanalysis/MERRA-2/ (last accessed on 20 April 2025)]. ERA5 data can be found here: [https://cds.climate.copernicus.eu/ (last accessed on 20 April 2025)]. CHAP data can be found here: [https://data.tpdc.ac.cn/home (last accessed on 20 April 2025)]. GDAS data can be found here: [https://www.ready.noaa.gov/ (last accessed on 20 April 2025)].

Acknowledgments: We sincerely thank the Google Earth Engine (GEE) platform for providing powerful data processing capabilities and Yaqiang Wang for providing software assistance.

Conflicts of Interest: The authors declare no conflicts of interest.

References

1. Seinfeld, J.H.; Bretherton, C.; Carslaw, K.S.; Coe, H.; DeMott, P.J.; Dunlea, E.J.; Feingold, G.; Ghan, S.; Guenther, A.B.; Kahn, R.; et al. Improving Our Fundamental Understanding of the Role of Aerosol−cloud Interactions in the Climate System. *Proc. Natl. Acad. Sci. USA* **2016**, *113*, 5781–5790. [CrossRef] [PubMed]
2. Zhao, C.; Sun, Y.; Yang, J.; Li, J.; Zhou, Y.; Yang, Y.; Fan, H.; Zhao, X. Observational Evidence and Mechanisms of Aerosol Effects on Precipitation. *Sci. Bull.* **2024**, *69*, 1569–1580. [CrossRef] [PubMed]
3. Froyd, K.D.; Yu, P.; Schill, G.P.; Brock, C.A.; Kupc, A.; Williamson, C.J.; Jensen, E.J.; Ray, E.; Rosenlof, K.H.; Bian, H.; et al. Dominant Role of Mineral Dust in Cirrus Cloud Formation Revealed by Global-Scale Measurements. *Nat. Geosci.* **2022**, *15*, 177–183. [CrossRef]
4. Li, Z.; Guo, J.; Ding, A.; Liao, H.; Liu, J.; Sun, Y.; Wang, T.; Xue, H.; Zhang, H.; Zhu, B. Aerosol and Boundary-Layer Interactions and Impact on Air Quality. *Natl. Sci. Rev.* **2017**, *4*, 810–833. [CrossRef]
5. Kok, J.F.; Ridley, D.A.; Zhou, Q.; Miller, R.L.; Zhao, C.; Heald, C.L.; Ward, D.S.; Albani, S.; Haustein, K. Smaller Desert Dust Cooling Effect Estimated from Analysis of Dust Size and Abundance. *Nat. Geosci.* **2017**, *10*, 274–278. [CrossRef]
6. Reid, J.P.; Bertram, A.K.; Topping, D.O.; Laskin, A.; Martin, S.T.; Petters, M.D.; Pope, F.D.; Rovelli, G. The Viscosity of Atmospherically Relevant Organic Particles. *Nat. Commun.* **2018**, *9*, 956. [CrossRef]
7. Mahowald, N.M.; Hamilton, D.S.; Mackey, K.R.M.; Moore, J.K.; Baker, A.R.; Scanza, R.A.; Zhang, Y. Aerosol Trace Metal Leaching and Impacts on Marine Microorganisms. *Nat. Commun.* **2018**, *9*, 2614. [CrossRef]
8. Pedde, M.; Larson, T.V.; D'Souza, J.; Szpiro, A.A.; Kloog, I.; Lisabeth, L.D.; Jacobs, D.; Sheppard, L.; Allison, M.; Kaufman, J.D.; et al. Coarse Particulate Matter and Markers of Inflammation and Coagulation in the Multi-Ethnic Study of Atherosclerosis (MESA) Population: A Repeat Measures Analysis. *Environ. Health Perspect.* **2024**, *132*, 027009. [CrossRef]
9. Li, R.; Wiedinmyer, C.; Hannigan, M.P. Contrast and Correlations between Coarse and Fine Particulate Matter in the United States. *Sci. Total Environ.* **2013**, *456–457*, 346–358. [CrossRef]
10. Middleton, N.J. Desert Dust Hazards: A Global Review. *Aeolian Res.* **2017**, *24*, 53–63. [CrossRef]
11. Todd, M.C.; Cavazos-Guerra, C. Dust Aerosol Emission over the Sahara during Summertime from Cloud-Aerosol Lidar with Orthogonal Polarization (CALIOP) Observations. *Atmos. Environ.* **2016**, *128*, 147–157. [CrossRef]
12. Isaza, A.; Kay, M.; Evans, J.P.; Bremner, S.; Prasad, A. Validation of Australian Atmospheric Aerosols from Reanalysis Data and CMIP6 Simulations. *Atmos. Res.* **2021**, *264*, 105856. [CrossRef]
13. Uno, I.; Eguchi, K.; Yumimoto, K.; Takemura, T.; Shimizu, A.; Uematsu, M.; Liu, Z.; Wang, Z.; Hara, Y.; Sugimoto, N. Asian Dust Transported One Full Circuit around the Globe. *Nat. Geosci.* **2009**, *2*, 557–560. [CrossRef]
14. Huang, J.; Wang, T.; Wang, W.; Li, Z.; Yan, H. Climate Effects of Dust Aerosols over East Asian Arid and Semiarid Regions. *J. Geophys. Res. Atmos.* **2014**, *119*, 11398–11416. [CrossRef]
15. Li, C.; Krotkov, N.A.; Dickerson, R.R.; Li, Z.; Yang, K.; Chin, M. Transport and Evolution of a Pollution Plume from Northern China: A Satellite-Based Case Study. *J. Geophys. Res. Atmos.* **2010**, *115*, D7. [CrossRef]

16. Liu, Y.; Zhu, Q.; Wang, R.; Xiao, K.; Cha, P. Distribution, Source and Transport of the Aerosols over Central Asia. *Atmos. Environ.* **2019**, *210*, 120–131. [CrossRef]
17. Zhu, Q.; Liu, Y.; Shao, T.; Tang, Y. Transport of Asian Aerosols to the Pacific Ocean. *Atmos. Res.* **2020**, *234*, 104735. [CrossRef]
18. Huang, X.; Ding, A.; Wang, Z.; Ding, K.; Gao, J.; Chai, F.; Fu, C. Amplified Transboundary Transport of Haze by Aerosol–Boundary Layer Interaction in China. *Nat. Geosci.* **2020**, *13*, 428–434. [CrossRef]
19. Pi, H.; Sharratt, B.; Lei, J. Atmospheric Dust Events in Central Asia: Relationship to Wind, Soil Type, and Land Use. *J. Geophys. Res. Atmos.* **2017**, *122*, 6652–6671. [CrossRef]
20. Shen, Y.-J.; Shen, Y.; Guo, Y.; Zhang, Y.; Pei, H.; Brenning, A. Review of Historical and Projected Future Climatic and Hydrological Changes in Mountainous Semiarid Xinjiang (Northwestern China), Central Asia. *CATENA* **2020**, *187*, 104343. [CrossRef]
21. Huang, J.; Minnis, P.; Yan, H.; Yi, Y.; Chen, B.; Zhang, L.; Ayers, J.K. Dust Aerosol Effect on Semi-Arid Climate over Northwest China Detected from A-Train Satellite Measurements. *Atmos. Chem. Phys.* **2010**, *10*, 6863–6872. [CrossRef]
22. Deng, X.; Xie, C.; Liu, D.; Wang, Y. Comparisons of Aerosol Types and Optical Characters over Shouxian Area China Observed from Ground- and Space-Based Systems. *Opt. Express* **2024**, *32*, 27081–27098. [CrossRef]
23. Xu, M.; Ding, J.; Liu, J.; Liu, F.; Jin, X.; Qu, Y. Vertical Distribution and Transport of Aerosols during a Dust Event in Xinjiang, Northwest China. *J. Meteorol. Res.* **2023**, *37*, 387–403. [CrossRef]
24. Ou, Y.; Li, Z.; Chen, C.; Zhang, Y.; Li, K.; Shi, Z.; Dong, J.; Xu, H.; Peng, Z.; Xie, Y.; et al. Evaluation of MERRA-2 Aerosol Optical and Component Properties over China Using SONET and PARASOL/GRASP Data. *Remote Sens.* **2022**, *14*, 821. [CrossRef]
25. Zhu, Z.; Li, H.; Fan, S.; Xu, W.; Fang, R.; Liu, B.; Gong, W. The Covariability between Temperature Inversions and Aerosol Vertical Distribution over China. *Atmos. Pollut. Res.* **2024**, *15*, 101959. [CrossRef]
26. Lu, X.; Mao, F.; Pan, Z.; Gong, W.; Wang, W.; Tian, L.; Fang, S. Three-Dimensional Physical and Optical Characteristics of Aerosols over Central China from Long-Term CALIPSO and HYSPLIT Data. *Remote Sens.* **2018**, *10*, 314. [CrossRef]
27. Chen, X.; Zuo, H.; Zhang, Z.; Cao, X.; Duan, J.; Zhu, C.; Zhang, Z.; Wang, J. Full-Coverage 250 m Monthly Aerosol Optical Depth Dataset (2000–2019) Amended with Environmental Covariates by an Ensemble Machine Learning Model over Arid and Semi-Arid Areas, NW China. *Earth Syst. Sci. Data* **2022**, *14*, 5233–5252. [CrossRef]
28. Ge, Y.; Abuduwaili, J.; Ma, L.; Wu, N.; Liu, D. Potential Transport Pathways of Dust Emanating from the Playa of Ebinur Lake, Xinjiang, in Arid Northwest China. *Atmos. Res.* **2016**, *178–179*, 196–206. [CrossRef]
29. Zhou, Y.; Gao, X.; Meng, X.; Lei, J.; Halik, Ü. Characteristics of the Spatio-Temporal Dynamics of Aerosols in Central Asia and Their Influencing Factors. *Remote Sens.* **2022**, *14*, 2684. [CrossRef]
30. Zhou, Q.; Li, J.; Xu, J.; Qin, X.; Deng, C.; Fu, J.S.; Wang, Q.; Yiming, M.; Huang, K.; Zhuang, G. First Long-Term Detection of Paleo-Oceanic Signature of Dust Aerosol at the Southern Marginal Area of the Taklimakan Desert. *Sci. Rep.* **2018**, *8*, 6779. [CrossRef]
31. Chen, S.; Huang, J.; Li, J.; Jia, R.; Jiang, N.; Kang, L.; Ma, X.; Xie, T. Comparison of Dust Emissions, Transport, and Deposition between the Taklimakan Desert and Gobi Desert from 2007 to 2011. *Sci. China Earth Sci.* **2017**, *60*, 1338–1355. [CrossRef]
32. Jia, R.; Li, J.; Zhu, Q.; Li, Y.; Tian, Y.; Li, Y.; Xu, Z. Three-Dimensional Distribution and Formation Causes of Aerosols over Northwest China. *J. Desert Res.* **2021**, *41*, 34–43.
33. Lyapustin, A.; Wang, Y.; Korkin, S.; Huang, D. MODIS Collection 6 MAIAC Algorithm. *Atmos. Meas. Tech.* **2018**, *11*, 5741–5765. [CrossRef]
34. Zhu, Z.; Zhang, Z.; Liu, F.; Chen, Z.; Ren, Y.; Guo, Q. Study on Accuracy Evaluation of MCD19A2 and Spatiotemporal Distribution of AOD in Arid Zones of Central Asia. *Sustainability* **2023**, *15*, 13959. [CrossRef]
35. Chen, X.; Ding, J.; Liu, J.; Wang, J.; Ge, X.; Wang, R.; Zuo, H. Validation and Comparison of High-Resolution MAIAC Aerosol Products over Central Asia. *Atmos. Environ.* **2021**, *251*, 118273. [CrossRef]
36. Winker, D.M.; Pelon, J.; Coakley, J.A.; Ackerman, S.A.; Charlson, R.J.; Colarco, P.R.; Flamant, P.; Fu, Q.; Hoff, R.M.; Kittaka, C.; et al. The CALIPSO Mission. *Bull. Am. Meteorol. Soc.* **2010**, *91*, 1211–1230. [CrossRef]
37. Randles, C.A.; da Silva, A.M.; Buchard, V.; Colarco, P.R.; Darmenov, A.; Govindaraju, R.; Smirnov, A.; Holben, B.; Ferrare, R.; Hair, J.; et al. The MERRA-2 Aerosol Reanalysis, 1980 Onward. Part I: System Description and Data Assimilation Evaluation. *J. Clim.* **2017**, *30*, 6823–6850. [CrossRef]
38. Hersbach, H.; Bell, B.; Berrisford, P.; Biavati, G.; Horányi, A.; Muñoz Sabater, J.; Nicolas, J.; Peubey, C.; Radu, R.; Rozum, I.; et al. ERA5 Hourly Data on Pressure Levels from 1979 to Present. *Copernic. Clim. Change Serv. (C3s) Clim. Data Store (Cds)* **2018**, *10*. [CrossRef]
39. Wei, J.; Li, Z. ChinaHigh PM 2.5: High-Resolution and High-Quality Ground-Level PM 2.5 Dataset for China (2000–2022). *Zenodo* **2019**, 6398971. [CrossRef]
40. Wei, J.; Li, Z.; Xue, W.; Sun, L.; Fan, T.; Liu, L.; Su, T.; Cribb, M. The ChinaHighPM10 Dataset: Generation, Validation, and Spatiotemporal Variations from 2015 to 2019 across China. *Environ. Int.* **2021**, *146*, 106290. [CrossRef]
41. Wang, Y.Q. MeteoInfo: GIS Software for Meteorological Data Visualization and Analysis. *Meteorol. Appl.* **2014**, *21*, 360–368. [CrossRef]

42. Draxler, R.R.; Hess, G. An Overview of the HYSPLIT_4 Modelling System for Trajectories. *Aust. Meteorol. Mag.* **1998**, *47*, 295–308.
43. Hsu, Y.-K.; Holsen, T.M.; Hopke, P.K. Comparison of Hybrid Receptor Models to Locate PCB Sources in Chicago. *Atmos. Environ.* **2003**, *37*, 545–562. [CrossRef]
44. Wang, Y.Q.; Zhang, X.Y.; Draxler, R.R. TrajStat: GIS-Based Software That Uses Various Trajectory Statistical Analysis Methods to Identify Potential Sources from Long-Term Air Pollution Measurement Data. *Environ. Model. Softw.* **2009**, *24*, 938–939. [CrossRef]
45. Polissar, A.V.; Hopke, P.K.; Harris, J.M. Source Regions for Atmospheric Aerosol Measured at Barrow, Alaska. *Environ. Sci. Technol.* **2001**, *35*, 4214–4226. [CrossRef]
46. Liu, J.; Ding, J.; Rexiding, M.; Li, X.; Zhang, J.; Ran, S.; Bao, Q.; Ge, X. Characteristics of Dust Aerosols and Identification of Dust Sources in Xinjiang, China. *Atmos. Environ.* **2021**, *262*, 118651. [CrossRef]
47. Gan, Y.; Zhang, Z.; Liu, F.; Chen, Z.; Guo, Q.; Zhu, Z.; Ren, Y. Analysis of Characteristics and Changes in Three-Dimensional Spatial and Temporal Distribution of Aerosol Types in Central Asia. *Sci. Total Environ.* **2024**, *927*, 172196. [CrossRef]
48. He, Q.; Gu, Y.; Zhang, M. Spatiotemporal Patterns of Aerosol Optical Depth throughout China from 2003 to 2016. *Sci. Total Environ.* **2019**, *653*, 23–35. [CrossRef]
49. van Donkelaar, A.; Martin, R.V.; Brauer, M.; Hsu, N.C.; Kahn, R.A.; Levy, R.C.; Lyapustin, A.; Sayer, A.M.; Winker, D.M. Global Estimates of Fine Particulate Matter Using a Combined Geophysical-Statistical Method with Information from Satellites, Models, and Monitors. *Environ. Sci. Technol.* **2016**, *50*, 3762–3772. [CrossRef]
50. Zhou, C.; Yang, X.; Liu, Y.; Zhu, Q.; Xie, Y.; Yang, F.; Ali, M.; Huo, W.; He, Q.; Meng, L. Terrain Effects of the Tibetan Plateau on Dust Aerosol Distribution over the Tarim Basin, China. *Atmos. Res.* **2024**, *298*, 107143. [CrossRef]
51. Chen, X.; Ding, J.; Wang, J.; Ge, X.; Raxidin, M.; Liang, J.; Chen, X.; Zhang, Z.; Cao, X.; Ding, Y. Retrieval of Fine-Resolution Aerosol Optical Depth (AOD) in Semiarid Urban Areas Using Landsat Data: A Case Study in Urumqi, NW China. *Remote Sens.* **2020**, *12*, 467. [CrossRef]
52. Campbell, J.R.; Tackett, J.L.; Reid, J.S.; Zhang, J.; Curtis, C.A.; Hyer, E.J.; Sessions, W.R.; Westphal, D.L.; Prospero, J.M.; Welton, E.J.; et al. Evaluating Nighttime CALIOP 0.532 μm Aerosol Optical Depth and Extinction Coefficient Retrievals. *Atmos. Meas. Tech.* **2012**, *5*, 2143–2160. [CrossRef]
53. Lv, F.; Yang, Y.; Yang, J. Spatiotemporal Distribution Characteristics and Relationship Analysis of Aerosol Optical Depth and PM2.5 Concentration: Taking the "2+26" Urban Agglomeration as an Example. *Acta Ecol. Sin.* **2023**, *43*, 153–165.
54. Aldabash, M.; Bektas Balcik, F.; Glantz, P. Validation of MODIS C6.1 and MERRA-2 AOD Using AERONET Observations: A Comparative Study over Turkey. *Atmosphere* **2020**, *11*, 905. [CrossRef]
55. Tao, M.; Chen, L.; Wang, J.; Wang, L.; Wang, W.; Lin, C.; Gui, L.; Wang, L.; Yu, C.; Wang, Y. Characterization of Dust Activation and Their Prevailing Transport over East Asia Based on Multi-Satellite Observations. *Atmos. Res.* **2022**, *265*, 105886. [CrossRef]
56. Ma, W.; Ding, J.; Jin, X. Spatial Heterogeneity and Driving Factors of Aerosol in Western China: Analysis on Multiangle Implementation of Atmospheric Correction–Aerosol Optical Depth in Xinjiang over 2001–2019. *Int. J. Climatol.* **2023**, *43*, 1993–2011. [CrossRef]
57. Li, J.; He, Q.; Ge, X.; Abbas, A.; Jin, L. Spatio-Temporal Changes of AOD in Xinjiang of China from 2000 to 2019: Which Factor Is More Influential, Natural Factor or Human Factor? *PLoS ONE* **2021**, *16*, e0253942. [CrossRef]

Disclaimer/Publisher's Note: The statements, opinions and data contained in all publications are solely those of the individual author(s) and contributor(s) and not of MDPI and/or the editor(s). MDPI and/or the editor(s) disclaim responsibility for any injury to people or property resulting from any ideas, methods, instructions or products referred to in the content.